

Long-term Variation of the Corona in Quiet Regions

S. Kamio¹ · J.T. Mariska²

© Springer ●●●

Abstract Using *Hinode* EUV Imaging Spectrometer (EIS) spectra recorded daily at Sun center from the end of 2006 to early 2011, we studied the long-term evolution of the quiet corona. The light curves of the higher temperature emission lines exhibit larger variations in sync with the solar activity cycle while the cooler lines show reduced modulation. Our study shows that the high temperature component of the corona changes in quiet regions, even though the coronal electron density remains almost constant there. The results suggest that heat input to the quiet corona varies with the solar activity cycle.

Keywords: Corona, Quiet – Solar Cycle, Observations – Spectral Line, Intensity and Diagnostics

1. Introduction

Radiation from the corona changes dramatically over the solar activity cycle. Peres *et al.* (2000) studied the long-term variation of the soft X-ray flux measured by *Yohkoh*/SXT (Tsuneta *et al.*, 1991) and found that the emission measure of the whole Sun changes by orders of magnitude between the solar activity maximum and the minimum. The irradiances of EUV coronal emission lines exhibit a large variation in sync with the solar cycle, with larger amplitude at the higher temperatures (Del Zanna and Andretta, 2011). Since the coronal irradiance is thought to be a measure of the magnetic activity of the whole corona, it is important to understand what features on the Sun cause the irradiance variation. The variation of the irradiance is mainly attributed to magnetic field concentrations associated with active regions, (*e.g.*, Foukal, 1990), however, Schühle *et al.* (2000) demonstrated that UV emission lines from the lower corona increased in quiet regions during the ascending phase of the solar activity cycle. Their results suggest that magnetic activity in quiet regions also changes with the solar cycle.

¹ Max-Planck-Institut für Sonnensystemforschung, 37191
Katlenburg-Lindau, Germany
email: skamio@spd.aas.org

² School of Physics, Astronomy, and Computational
Sciences, George Mason University, 4400 University Drive,
Fairfax, VA 22030, USA

To quantify the variation in quiet regions, coronal emission lines formed at high temperatures need to be studied. We investigate the long-term variation of the EUV radiance recorded daily at Sun center by the EUV Imaging Spectrometer (EIS; Culhane *et al.*, 2007) aboard *Hinode* (Kosugi *et al.*, 2007). The paper is organized as follows; the data reduction and calibration procedure are described in Section 2. The long-term variation of emission lines and electron density estimation are presented in Section 3. The results and interpretations are discussed in Section 4.

2. Data Reduction

The EIS SYNOP001 and SYNOP005 studies are regular observational programs recording EUV spectra near Sun center on a daily basis. Since the Sun is rotating at a rate of 28 days near the equator, the time series smoothed over the rotation period provides average properties of the corona near Sun center. However, one of the challenges in determining a long-term variation of the corona is that the sensitivity of EIS gradually decreases with time.

A detailed study of the EIS sensitivity change was carried out by using the He II $\lambda 256.32 \text{ \AA}$ emission line recorded using the regular quiet region observation studies SYNOP002 and SYNOP006 near disk center (Mariska 2012, private communication). Those data suggest that the degradation of the EIS sensitivity can be expressed as

$$e = \{\exp(t/\tau_1) + \exp(t/\tau_2)\}/2, \quad (1)$$

where t denotes the time from *Hinode* launch on 22 September 2006, and the e -folding times τ_1 and τ_2 are 467 days and 11311 days, respectively. In this study, the degradation of the EIS sensitivity is compensated for using Equation (1).

A large number of individual emission line profile fits go into each averaged data point used to compute the sensitivity correction, and there are many possible ways to estimate the error in each averaged data point. Two obvious choices are to weight each averaged data point by the number of individual measurements that went into its determination or to weight each point by the standard deviation of all the data points that went into the average. Each weighting results in nearly the same results for the initial intensity and the time constant for the shorter decay time, but different answers for the longer decay constant. The errors for the fits, however, are nearly the same: less than 5% for the initial intensity, about 15% for the shorter decay constant, and about 40% for the longer decay constant. The error for the longer decay constant is larger because the value itself is large—several decades. Thus the trend is very small over the time interval of the data fitted in this study.

The radiance of the spectral lines listed in Table 1 is deduced by fitting a Gaussian function to the spectrum integrated over 100 arcsec in the north-south direction along the slit. This integration along the slit is intended to improve the signal to noise ratio of the spectrum and to smooth out small-scale structures, such as coronal bright points, along the slit. The spatial extent in east-west

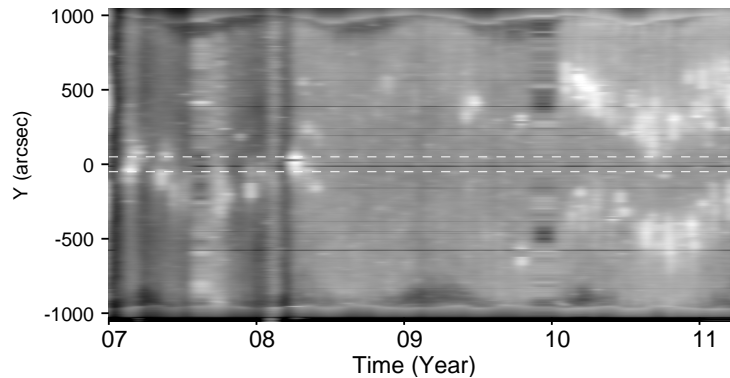


Figure 1. Time series of X-ray flux along the central meridian. Dashed lines in the middle mark the region studied with EIS.

direction is 1 arcsec since the spectrum is recorded with 1 arcsec wide slit. These emission lines exhibit sufficient counts in quiet regions for a useful analysis. After correcting for the long-term degradation of the EIS sensitivity denoted by Equation (1), data number (DN) is converted to physical units ($\text{erg cm}^{-2} \text{s}^{-1} \text{sr}^{-1}$) by using the pre-flight calibration of the EIS effective area (Lang *et al.*, 2006; Culhane *et al.*, 2007), which is provided in the EIS branch of Solar Software (SSW).

The light curve for each emission line is further smoothed along the temporal axis by convolving it with a Gaussian function with a full width at half maximum (FWHM) of 28 days—the solar rotation period. This is intended to suppress the radiance variation caused by the appearance and disappearance of any small active regions during a solar rotation (Woods and Rottman, 2005). The smoothing process at a time t_0 is performed by convolving with a Gaussian weighting function

$$a = \exp\left(-\frac{(t - t_0)^2}{2\sigma^2}\right), \quad (2)$$

where $\text{FWHM} = 2\sqrt{2\log 2}\sigma$.

3. Results

3.1. Location of Active Regions

To make sure that the EIS observations at Sun center are not directly influenced by active regions, we constructed a time-space map by lining up stripes of central meridian data in daily images obtained by the X-Ray Telescope (XRT; Golub *et al.*, 2007) on *Hinode*. Figure 1 shows a time-space map composed of data obtained with either the Al_{poly} or Al_{mesh} filters, which are available for most of the period. Since the temperature responses of these two filters are almost identical above 2 MK (Golub *et al.*, 2007), the appearance of active regions in these filters should be quite similar. The time-space map is smoothed along the

Table 1. Fitted radiance at the beginning of *Hinode* observations (December 2006) and at the minimum (February 2009).

| Ion | λ [Å] | $\log T_e$ [K] | Dec 2006 [erg cm ⁻² s ⁻¹ sr ⁻¹] | Feb 2009 | Ratio |
|---------------------|------------------|-------------------|--|----------|-------|
| Fe XIV ¹ | 264.79 | 6.25 | 38 | 7.8 | 4.8 |
| Fe XIII | 202.04 | 6.20 | 207 | 33 | 6.2 |
| Fe XII | 193.51 | 6.15 | 225 | 70 | 3.2 |
| Si X | 258.37 | 6.15 | 75 | 35 | 2.1 |
| Fe XI | 180.40 | 6.10 | 426 | 282 | 1.5 |
| Fe X | 184.54 | 6.00 | 103 | 118 | 0.86 |
| Si VII | 275.36 | 5.80 | 16 | 23 | 0.71 |
| Fe VIII | 185.21 | 5.65 | 31 | 44 | 0.72 |
| He II | 256.32 | 4.85 | 256 | 229 | 1.1 |

¹With a blending Fe XI 264.77Å

temporal axis by convolving it with the Gaussian weighting function denoted by Equation (2). The pixel size in north-south direction remains at 2 arcsec.

The region recorded by the EIS observations is indicated with horizontal dashed lines. Active regions passing the meridian appear as bright features in the plot. Note that the EIS data are always recorded at Sun center viewed from the Earth, and the tilt of the solar rotation axis is not compensated for. Active regions occasionally appeared near Sun center from 2007 to the middle of 2008, while they are almost absent in 2009. In 2010, they again started to appear regularly, but distant from Sun center. The plot demonstrates that with only one exception in 2008 the EIS observing region is not covered by active regions. Therefore, the radiances deduced from the EIS observations are not directly affected by an increase or a decrease in the number of active regions.

3.2. EUV Radiance Variation

Figure 2 shows the smoothed light curve in each emission line. The measured radiance is smoothed by convolving with a Gaussian function with a width of the 28-day solar rotation period (see Section 2). Since the light curves are nearly symmetric with respect to the minimum in 2009, the smoothed radiance is fitted with a second-order polynomial function to determine the long-term variation. The fitted polynomial functions are overplotted using dotted curves in Figure 2, and show a reasonable agreement with the light curves. In the following, the radiance in each emission line is determined by using the fitted polynomial functions. The lowest radiance for Fe XII is attained in February 2009, which is regarded as the minimum of the long-term variation. (The NOAA Space Weather Prediction Center lists the solar cycle minimum date as December 2008.) The radiance values at the beginning of *Hinode* observations (December 2006) and at the minimum (February 2009) are summarized in Table 1.

Emission lines hotter than Fe X tend to show larger variation ratios with increasing temperature. The only exception is the Fe XIV line, which has a smaller

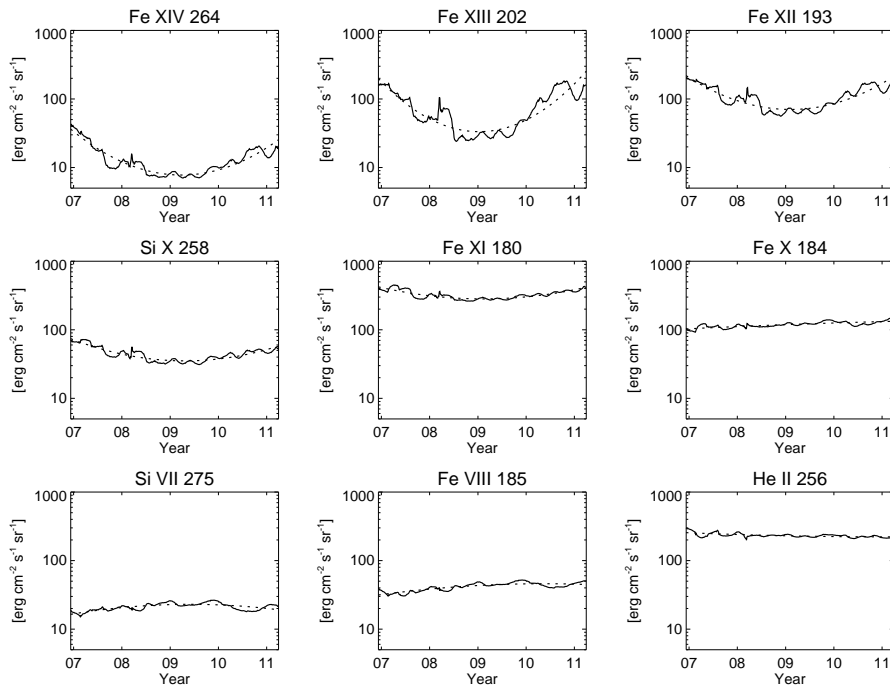


Figure 2. Radiances measured in different emission lines are plotted as solid curves. The dotted curve in each panel show a second-order polynomial fit to the measured radiance.

ratio than that of the Fe XIII line. A possible effect of a blending emission line is discussed in Section 3.5. On the contrary, the low-temperature emission lines between Fe VIII and Fe X show constant or a slightly larger radiance at the minimum. Although the sensitivity change is determined from the He II emission line alone, a wavelength dependent degradation of the instrument is not likely the reason for this trend, because Fe VIII and Si VII are observed in different EIS wavelength channels and yet exhibit a similar variation (Table 1).

3.3. Spatial Distribution of the Radiance

To study the spatial distribution of the radiance, Figure 3 compares the histogram of the Fe XII $\lambda 193.51\text{\AA}$ radiance in each pixel of EIS recorded in December 2006 and in February 2009. The intense Fe XII $\lambda 193.51\text{\AA}$ emission line allows us to analyze the radiance in an individual pixel ($1'' \times 1''$) without summing, which can differentiate between localized and dispersed brightenings. The histogram is peaked at $200 \text{ erg cm}^{-2} \text{ s}^{-1} \text{ sr}^{-1}$ in the December 2006 data (solid line), while that in February 2009 is at $60 \text{ erg cm}^{-2} \text{ s}^{-1} \text{ sr}^{-1}$ (dotted line). The ratio of these values is close to the mean radiance ratio of 3.2 in Table 1. The histogram demonstrates that the long-term variation of the average radiance is not caused by an increase or a decrease of localized bright features, but instead by a variation of the entire region.

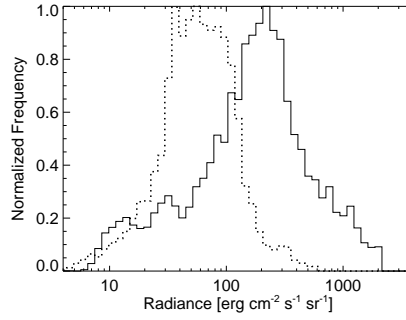


Figure 3. Histogram of the Fe XII $\lambda 193.51\text{\AA}$ radiance. Solid and dotted lines show the distributions in the December 2006 data and in the February 2009 data, respectively.

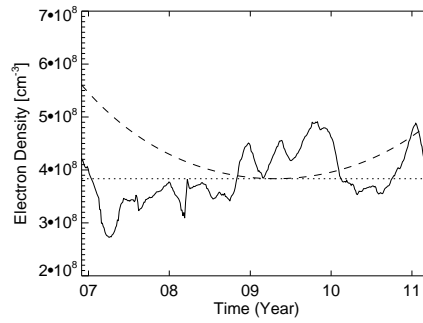


Figure 4. Time history of the electron density derived from the Si x line pair.

3.4. Electron Density

The electron density is estimated from the line ratio of Si x $\lambda 258.37\text{\AA}/261.04\text{\AA}$. The line ratio is deduced from the Si x radiance integrated over 100 arcsec along the slit. The relationship between electron density and the line ratio is calculated using version 7.1 of the CHIANTI atomic database (Dere *et al.*, 1997; Landi *et al.*, 2012). Figure 4 presents the electron density variation. The obtained electron density is smoothed along the temporal axis in the same manner as the radiance in Section 3.2. The dotted line plotted over Figure 4 indicates a constant density of $3.8 \times 10^8\text{ cm}^{-3}$. In contrast to the radiance variation in the Si x emission line, the electron density shows no clear trend of solar cycle variation. The uncertainty of the radiance due to the spectrum fitting is estimated to be smaller than 10%, which corresponds to an uncertainty of 30% in the density estimation. Note that the line ratio analysis depends solely on the relative radiance and is not affected by the uncertainty of the absolute radiance.

In the case of an isothermal plasma, the observed radiance I is denoted as

$$I = f n_e^2 g(T, n_e) \quad (3)$$

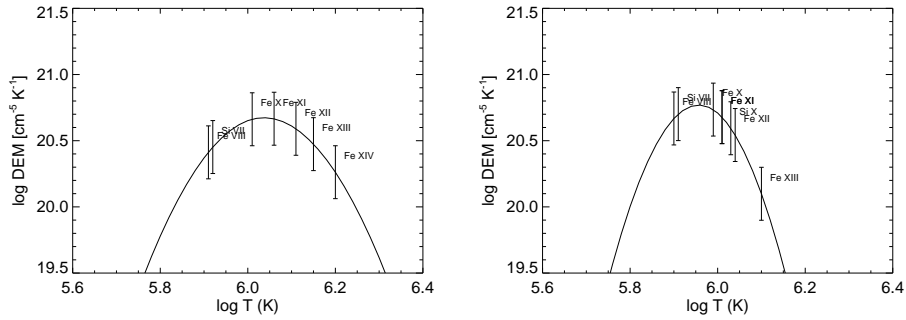


Figure 5. Results from DEM analysis in December 2006 (left panel) and February 2009 (right panel).

where f , d , and $g(T, n_e)$ are the filling factor of the emitting plasma, the depth over which the emission line is formed, and the contribution function to the line, respectively. To examine whether the density variation is responsible for the radiance variation, a square root of the Si x $\lambda 258.37\text{\AA}$ radiance is overplotted in Figure 4 with a dashed curve. If the density variation is the primary cause of radiance variation, the density should agree with the square root of radiance. Figure 4 indicates that the density variation is not sufficient to reproduce the observed radiance variation. Other factors, the filling factor f , depth of the corona d , or the contribution function, are thus responsible for the radiance variation.

3.5. DEM Analysis

A differential emission measure (DEM) analysis is carried out with the aid of the CHIANTI atomic database. All emission lines in Table 1 except for He II are used in the analysis. Since a sufficient number of emission lines are available only within a temperature range of $\log T_e = 5.65\text{--}6.25$, we restrict the analysis to that interval. A DEM in that temperature range is computed by using the procedure provided in the CHIANTI atomic database. It deduces an optimum DEM so that the DEM multiplied by the contribution function of each emission line reproduces the measured radiance. Figure 5 presents the DEM at two different times. In December 2006, the DEM peak is located at $\log T_e = 6.05$, while that at the minimum in February 2009 the peak is found at 5.95. The high temperature tail of the DEM is extended higher in the former period than the minimum period. This explains the trend that the higher temperature emission lines exhibit greater decreases in the minimum period (Figure 2). In contrast, the lower temperature emission lines (Fe VIII and Si VII) indicate slight increases in the minimum period as the DEM peak is shifted towards the lower temperature. These results show that the properties of the quiet region corona change with the solar activity cycle.

The radiance in the Fe XIV $\lambda 264.79\text{\AA}$ line is a special case. It turns out that the radiance of Fe XIV $\lambda 264.79\text{\AA}$ is overtaken by a blending Fe XI $\lambda 264.77\text{\AA}$ feature during the minimum period. According to the CHIANTI estimation of

the radiance, Fe XIV is five times larger than Fe XI in December 2006, while Fe XIV gets smaller than Fe XI at the minimum in February 2009. Because of the Fe XI $\lambda 264.77 \text{ \AA}$ blending, the measured radiance at $\lambda 264.79 \text{ \AA}$ (Table 1) does not decrease much, resulting in a smaller variation than the Fe XIII $\lambda 202.04 \text{ \AA}$ light curve. Thus care should be taken in analyzing the Fe XIV $\lambda 264.79 \text{ \AA}$ radiance.

4. Discussion

We found a long-term variation of the EUV emission lines in quiet regions in sync with the solar activity cycle. The time series of the EIS spectra was recorded at Sun center, where there is minimal contamination from active regions (Figure 1). The light curves of emission lines above 1 MK clearly show that the quiet region corona varies with the solar activity cycle (Figure 2). The radiance variation is attributed to the coronal temperature rather than the coronal electron density. As shown in Figure 4, the observed density variation is inadequate to reproduce the observed radiance variation. The temperature dependent variation of the light curves is explained as a modulation of the high temperature component in the corona (Figure 5).

Orlando, Peres, and Reale (2001) claimed that the average temperature of low X-ray flux regions observed by the *Yohkoh*/SXT remained constant around 1.5 MK between the solar maximum and the minimum. A possible explanation for this disagreement is that the sensitivity of SXT is low below 1 MK, and hence is not optimum for diagnosing the corona around 1 MK. The EIS observations provided us with several emission lines at that temperature to allow a more detailed study.

Our study proves that the corona in quiet regions is not constant, but changes with the solar activity cycle. It suggests that the heat input to the quiet corona changes with the solar activity cycle. In addition, the spatial distribution of the radiance indicates that the radiance variation in the quiet region is a dispersed phenomenon rather than localized features (Figure 3). Since a nearly linear relationship has been established between total magnetic flux and X-ray radiance in quiet regions, active regions, and stars (Pevtsov *et al.*, 2003), our finding of coronal radiance variation is attributed to a change in total magnetic flux in the quiet region. Close *et al.* (2003) argued that quiet regions are filled with short loops connecting magnetic flux fragments in the photosphere, forming the so-called magnetic carpet. We speculate that the total magnetic flux of the small-scale magnetic loops in the corona changes with the solar activity cycle, and hence the heat input to the corona. Indeed, Pauluhn and Solanki (2003) studied magnetograms obtained in the quiet regions by SOHO/MDI and found that the fraction of network area increased from 10% near the solar activity minimum to 13% near the maximum. The long-term variation of magnetic fields in the corona needs to be studied in order to understand the coronal heating process in quiet regions. Our results should encourage modellers to consider how the small-scale magnetic fields in quiet regions are related to the solar activity cycle on a global scale. It must be noted that our observations covers only five years around the solar minimum. Therefore, the variation amplitude along the solar cycle remains to be studied when the solar maximum is reached.

Acknowledgements *Hinode* is a Japanese mission developed and launched by ISAS/JAXA, with NAOJ as domestic partner and NASA and STFC (UK) as international partners. It is operated by these agencies in co-operation with ESA and NSC (Norway). JTM acknowledges support from the NASA *Hinode* contract with the Naval Research Laboratory.

References

- Close, R.M., Parnell, C.E., Mackay, D.H., Priest, E.R.: 2003, *Solar Phys.* **212**, 251.
- Culhane, J.L., Harra, L.K., James, A.M., Al-Janabi, K., Bradley, L.J., Chaudry, R.A., Rees, K., Tandy, J.A., Thomas, P., Whillock, M.C.R., Winter, B., Doschek, G.A., Korendyke, C.M., Brown, C.M., Myers, S., Mariska, J., Seely, J., Lang, J., Kent, B.J., Shaughnessy, B.M., Young, P.R., Simnett, G.M., Castelli, C.M., Mahmoud, S., Mapson-Menard, H., Probyn, B.J., Thomas, R.J., Davila, J., Dere, K., Windt, D., Shea, J., Hagood, R., Moye, R., Hara, H., Watanabe, T., Matsuzaki, K., Kosugi, T., Hansteen, V., Wikstol, Ø.: 2007, *Solar Phys.* **243**, 19.
- Del Zanna, G., Andretta, V.: 2011, *Astron. Astrophys.* **528**, A139.
- Dere, K.P., Landi, E., Mason, H.E., Monsignori Fossi, B.C., Young, P.R.: 1997, *Astron. Astrophys. Suppl.* **125**, 149.
- Foukal, P.: 1990, *Phil. Trans. Roy. Soc. London* **330**, 591.
- Golub, L., Deluca, E., Austin, G., Bookbinder, J., Caldwell, D., Cheimets, P., Cirtain, J., Cosmo, M., Reid, P., Sette, A., Weber, M., Sakao, T., Kano, R., Shibasaki, K., Hara, H., Tsuneta, S., Kumagai, K., Tamura, T., Shimojo, M., McCracken, J., Carpenter, J., Haight, H., Siler, R., Wright, E., Tucker, J., Rutledge, H., Barbera, M., Peres, G., Varisco, S.: 2007, *Solar Phys.* **243**, 63.
- Kosugi, T., Matsuzaki, K., Sakao, T., Shimizu, T., Sone, Y., Tachikawa, S., Hashimoto, T., Minesugi, K., Ohnishi, A., Yamada, T., Tsuneta, S., Hara, H., Ichimoto, K., Suematsu, Y., Shimojo, M., Watanabe, T., Shimada, S., Davis, J.M., Hill, L.D., Owens, J.K., Title, A.M., Culhane, J.L., Harra, L.K., Doschek, G.A., Golub, L.: 2007, *Solar Phys.* **243**, 3.
- Landi, E., Del Zanna, G., Young, P.R., Dere, K.P., Mason, H.E.: 2012, *Astrophys. J.* **744**, 99.
- Lang, J., Kent, B.J., Paustian, W., Brown, C.M., Keyser, C., Anderson, M.R., Case, G.C.R., Chaudry, R.A., James, A.M., Korendyke, C.M., Pike, C.D., Probyn, B.J., Rippington, D.J., Seely, J.F., Tandy, J.A., Whillock, M.C.R.: 2006, *Appl. Opt.* **45**, 8689.
- Orlando, S., Peres, G., Reale, F.: 2001, *Astrophys. J.* **560**, 499.
- Pauluhn, A., Solanki, S.K.: 2003, *Astron. Astrophys.* **407**, 359.
- Peres, G., Orlando, S., Reale, F., Rosner, R., Hudson, H.: 2000, *Astrophys. J.* **528**, 537.
- Pevtsov, A.A., Fisher, G.H., Acton, L.W., Longcope, D.W., Johns-Krull, C.M., Kankelborg, C.C., Metcalf, T.R.: 2003, *Astrophys. J.* **598**, 1387.
- Schühle, U., Wilhelm, K., Hollandt, J., Lemaire, P., Pauluhn, A.: 2000, *Astron. Astrophys.* **354**, L71.
- Tsuneta, S., Acton, L., Bruner, M., Lemen, J., Brown, W., Carvalho, R., Catura, R., Freeland, S., Jurcevich, B., Owens, J.: 1991, *Solar Phys.* **136**, 37.
- Woods, T.N., Rottman, G.: 2005, *Solar Phys.* **230**, 375.

